Spontaneous self-assembly and structure of perfluoroalkylalkane surfactant hemimicelles by molecular dynamics simulations

Gonçalo M. C. Silva[a], Pedro Morgado[a], Pedro Lourenço[a,b], Michel Goldmann[b,c], and Eduardo J. M. Filipe[a,1]

[a]Centro de Química Estrutural, Instituto Superior Técnico, Universidade de Lisboa, 1049-001 Lisboa, Portugal; [b]Institut des NanoSciences de Paris, UMR 7588 CNRS, Sorbonne Université, 75252 Paris Cedex 05, France; and [c]Synchrotron SOLEIL, L'Orme des Merisiers, Saint Aubin, BP48 91192 Gif sur Yvette Cedex, France

Edited by Peter J. Rossky, Rice University, Houston, TX, and approved June 10, 2019 (received for review April 25, 2019)

Fully atomistic molecular-dynamics (MD) simulations of perfluoroalkylalkane molecules at the surface of water show the spontaneous formation of aggregates whose size and topography closely resemble the experimentally observed hemimicelles for this system. Furthermore, the grazing incidence X-ray diffraction (GIXD) pattern calculated from the simulation trajectories reproduces the experimental GIXD spectra previously obtained, fully validating the MD simulation results. The detailed analysis of the internal structure of the aggregates obtained by the MD simulations supports a definite rational explanation for the spontaneous formation, stability, size, and shape of perfluoroalkylalkane hemimicelles at the surface of water.

Langmuir films | perfluoroalkylalkanes | hemimicelles | molecular dynamics | self-assembly

Perfluoroalkylalkanes (PFAA, $C_nF_{2n+1}C_mH_{2m+1}$ or FnHm) are diblock copolymers in which an alkyl and a perfluoroalkyl segment are covalently bonded to form a single semifluorinated chain. Given the well-known "mutual phobicity" between hydrogenated and fluorinated chains, these molecules possess the "dual character" of amphiphilic molecules and the orientational ordering physics of smectogenic liquid crystals. PFAA are thus expected to display interesting interfacial behavior and the ability to self-assemble, either in pure form or in solvents selective to one of the segments. Indeed, PFAA are known to form a diversity of supramolecular nanostructures such as micelles, reverse micelles (1), smectic (layered) liquid crystalline phases (2–5), mesophases, etc., all of which are potential candidates for numerous applications, from medicine (6–12) to smart materials and tailored interfaces (13–17). Organization in the solid state in layered structures has also been described (18–21). The simultaneous presence of the mutually phobic hydrogenated and perfluorinated segments dramatically influences the structure of the fluid or material, inducing different forms of organization. An in-depth understanding of the underlying physics is of clear importance, both for developing the various applications and for fundamental reasons. Surface tension, for example, is a key property in the recently suggested use of PFAA as liquid ventilation excipients for nebulized drug delivery (22).

It should be realized, however, that unlike common hydrophilic/hydrophobic surfactants, in which one of the driving forces for organization is the strong interaction between polar or ionic groups and water, the amphiphilic nature of FnHm is the result of a subtle balance between weak and even weaker dispersion forces, a point which has earned these compounds the label of "primitive surfactants" (23).

Perhaps the most striking example of their surfactant character is the ability of FnHm to form stable Langmuir films at the air–water interface, despite the absence of a hydrophilic head group. Surprisingly, these Langmuir films are not homogeneous at the molecular scale, but highly organized systems formed by self-assembled arrays of typically monodispersed aggregates or hemimicelles with diameters ranging roughly from 30 to 60 nm, depending on the relative chain length of the hydrogenated and fluorinated segments. These domains were first observed at the surface of solid substrates by atomic force microscopy (AFM) (24–28) and later confirmed directly on liquid subphase by grazing incidence small angle X-ray diffraction (GISAXS) (29–31) experiments. Different hemimicelle morphologies have been observed, from circular to elongated and either pit- or tip-centered (32).

The structure and formation of PFAA hemimicelles has been a subject of debate over the years. Despite all efforts, the principles governing their origin and structure are yet to be understood. Their formation at zero surface pressure and resistance to coalescence even under strong compression are particularly puzzling (33–36). Indeed, it is not at all clear why PFAA monolayers are not uniform, especially considering their size and aggregation number, which is estimated to be on the order of a few thousands of molecules. Tentative explanations are blurred by the diversity of morphologies observed. To the best of our knowledge, very few attempts have been made to describe the phenomenon theoretically or computationally.

Semenov et al. (37) developed a 2D theoretical model of the FnHm monolayers, which takes into account dispersion and

Significance

Semifluorinated alkanes surfactants spontaneously form nanostructured Langmuir films at the surface of water, consisting of highly organized arrays of hemimicelles. These supramolecular nanostructures are potential candidates for numerous applications, from smart materials to medical devices. Despite all efforts, the principles governing the formation and structure of these hemimicelles are not understood. Atomistic molecular-dynamics (MD) simulations show the spontaneous formation of such aggregates strikingly resembling those experimentally observed, supporting a rational explanation for the formation, size and shape of the hemimicelles. The simulated grazing incidence X-ray diffraction spectrum matches that obtained experimentally, fully validating the MD results. Given the simplicity of these "primitive" amphiphiles compared with the common hydrophilic/hydrophobic surfactants, these results can contribute to understand self-assembly processes in general.

Author contributions: P.M., M.G., and E.J.M.F. designed research; G.M.C.S. and P.L. performed research; G.M.C.S., P.M., P.L., M.G., and E.J.M.F. analyzed data; and M.G. and E.J.M.F. wrote the paper.

The authors declare no conflict of interest.

This article is a PNAS Direct Submission.

[1]To whom correspondence may be addressed. Email: efilipe@tecnico.ulisboa.pt.

This article contains supporting information online at www.pnas.org/lookup/suppl/doi:10.1073/pnas.1906782116/-/DCSupplemental.

Published online July 5, 2019.

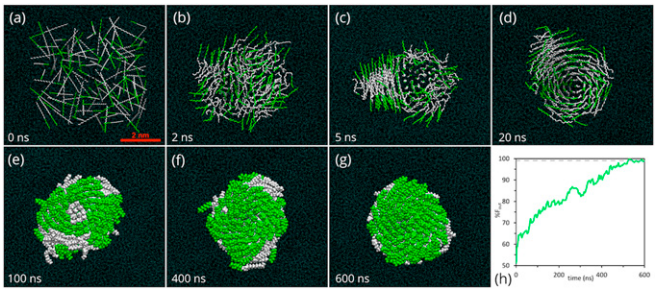

Fig. 1. Top-view snapshots of time evolution of a simulation of 100 F8H16 molecules at the surface of water: (*A*) initial randomly generated configuration; (*B* and *C*) formation of block domains; (*D*) merging of block domains; (*E* and *F*) gradual flipping of F8H16 molecules; (*G*) final configuration after 600 ns with all perfluoroalkyl chains oriented upwards in relation to the surface; (*F*) Evolution of orientation of F8H16 molecules. Fluorinated and hydrogenated segments are dyed green and white, respectively.

dipolar interactions and where the water subphase is treated as a structureless supporting surface. The model is able to predict the formation of aggregates emerging as a result of liquid/liquid phase separation in the Langmuir layer. Also according to the model, at low surface density the FnHm molecules would lie parallel to the interface and under compression would stand up via a first-order phase transition. In the vertical higher-density phase the molecules would form domains stabilized by electrostatic interactions, which are mainly due to the vertical dipole moments of the CF2–CH2 bonds. Interactions between these domains' dipoles are believed to limit growth and prevent coalescence. The proposed model is thus able to describe a number of features of the FnHm films, but predicts others, which have not been confirmed by experiments such as the predicted phase transition between the parallel and vertical phases. The model also does not account for the observed differences of stability and morphologies of the domains, which depend on molecular architecture and on the nature of the substrates. This latter factor is known to be crucial to the formation of domains. Indeed, hemimicelles have been obtained at the surface of water (30), mica (38), wet silicon wafers (30, 39), liquid crystals (40), and amphiphilic block copolymers (25). Conversely, no evidence of nanostructuring was observed at the surface of bulk FnHm liquids (41) or on dry silicon wafers (39). Similarly, the upper layer of collapsed FnHm films is not structured, contrarily to the first layer remaining in contact with water (33, 35). These results clearly demonstrate the importance of rigorously describing the interactions between FnHm molecules and also between these and the different substrates, particularly with water.

More recently, Piñeiro et al. (42), using MD simulations, predicted the formation of elongated micelles of F6H16 and F6H10 at the air/water interface. While hemimicelles of F6H16 and F6H10 have not been experimentally observed, the size and shape of the obtained aggregates is very different from those observed for the larger FnHm molecules. It should be explained that the adopted force field is a nonatomistic model that more importantly does not include electrostatic forces. We have shown in previous works the importance of taking into account the dipolar interactions between FnHm molecules and with water (43, 44). Additionally, the formation of cylindrical micelles could be an artifact resulting from the small size of the simulation box and by the small number of PFAA molecules, which is more than one order of magnitude below that found in experimentally observed hemimicelles for other FnHm.

In recent years we have accomplished a systematic experimental, computational, and theoretical study on the thermophysical properties of liquid PFAA, either pure or mixed with alkanes, perfluoroalkanes, and water. We have reported a number of properties of pure liquid PFAA [liquid density (45, 46), vapor pressure (43), viscosity (47), and surface tension (48)] and their mixtures [partial molar volume at infinite dilution (49, 50), solubility of water, and interfacial tension (44)] as a function of temperature, pressure, and relative length of the hydrogenated and fluorinated segments. These results were crucial for developing, parameterizing, and testing molecular models and force fields to be used in computer simulations and molecular-based theoretical calculations. Using different models, we have consistently shown that

1) For fluids involving hydrogenated and fluorinated chains, a simultaneous reduction of the dispersive interactions and an increase of the repulsive part of the intermolecular potential between hydrogenated and fluorinated segments is essential to reproduce both the enthalpic and volumetric properties displayed by these systems (48, 51, 52).
2) Structural factors, such as the rigidity of fluorinated chains, as opposed to the characteristic flexibility of hydrogenated, and the different cross-sections of the hydrogenated and fluorinated segments, also contribute to the observed behavior.
3) For PFAA we have been able to demonstrate the importance of the dipole and its impact on the properties of the pure fluid, such as vapor pressure, as well as on the interaction of PFAA with water.

In this work, building on our accumulated experience on modeling (using both theoretical approaches and molecular simulations) the properties and phase equilibria of fluorinated fluids, including PFAA and their mixtures with hydrogenated species, we performed MD simulations using a fully atomistic force field of varying numbers of F8H16 molecules at the surface of water, at very low surface density.

The simulations successfully show the spontaneous formation of circular aggregates whose size and topography strikingly resemble the experimentally observed structures.

Moreover, the grazing incidence X-ray diffraction (GIXD) pattern calculated from the simulation trajectories reproduces the experimental spectra previously obtained, fully validating the MD simulation results.

The detailed analysis of the structure of aggregates of different sizes, as obtained by MD simulation, supports a definite rational explanation for the spontaneous formation of PFAA hemimicelles at the surface of water at zero surface pressure.

Results and Discussion

As previously described, we performed atomistic MD simulations of different number of F8H16 molecules at the surface of water. Systems comprising up to 2,500 molecules have been simulated. The surface density was kept very low (~83 Å^2 molecule^{-1} for the 100 F8H16 system), corresponding to zero surface pressure. The initially randomly oriented F8H16 molecules spontaneously self-assembled into circular aggregates or hemimicelles (Fig. 1).

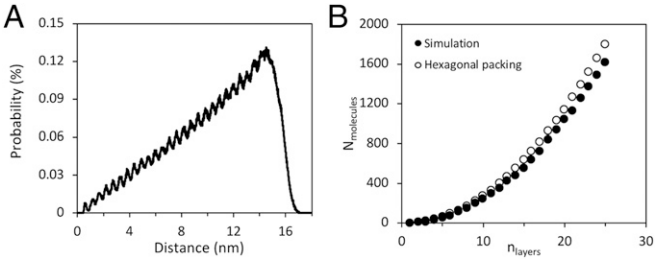

Fig. 2. (*A*) Ring distribution of F8H16 molecules within a 2,500-molecules aggregate relatively to the center of the aggregate. (*B*) Comparison of the packing observed in the simulations and the perfect hexagonal packing.

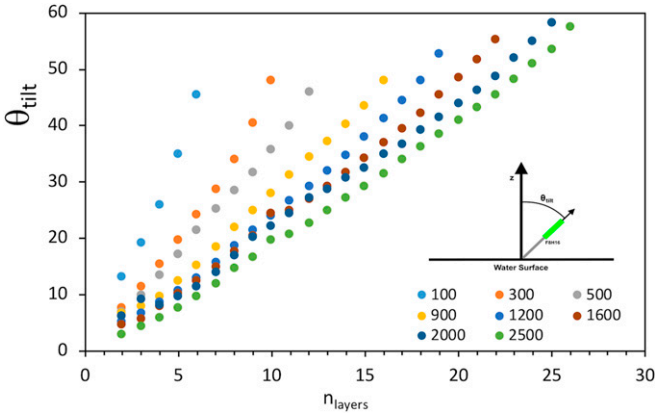

Fig. 3. F8H16 orientation: Tilting angle as a function of micelle size and distance to the center of the aggregate. (*Inset*) Definition of the tilting angle in the radial direction between the end-to-end vector of the F8H16 molecule and the z axis. Fluorinated and hydrogenated segments are dyed green and gray, respectively.

In the initial stages of the simulation, groups of molecules locally arranged into solid-like block structures (see Fig. 1 at 5 ns) with a quasihexagonal packing of parallel F8H16 chains. These domains, already clearly displaying segregation of the fluorocarbon and hydrocarbon moieties, then merged and formed single circular aggregates. Over time, molecules gradually changed orientation until all perfluoroalkyl segments were oriented upwards. For a system of 100 F8H16 molecules it took ~600 ns until all perfluoroalkyl segments were oriented toward the gaseous phase. Several factors contribute to the observed reorganization of orientations: hydrogenated chains are less hydrophobic and thus have lower interfacial tension with water than fluorinated chains; perfluorocarbons have lower surface tensions than hydrocarbons; the interactions between hydrocarbons and perfluorocarbons are weaker than expected, which induces segregation. Experimental X-ray (24, 25) and neutron reflectivity (53) and Kelvin surface potential (54) results are in agreement with the full fluorocarbon chain arrangement toward the air interface.

A close inspection of the structure of the aggregates reveals that

1) The F8H16 molecules are arranged in circular concentric rings, in almost hexagonal packing. The separation between consecutive rings is very well defined and on the order of 0.5 nm (Fig. 2*A*). As can be seen in Fig. 2*B*, the number of molecules within each ring, N, falls a bit short compared with that of a perfect hexagonal packing, $N = 3n(n-1)+1$, where n is the number of rings. The discrepancy results from the occasional occurrence of defects, the mobility of the molecules, and, as mentioned above, the fact that the aggregate is not flat. At the periphery, due to lack of cohesion, the aggregate becomes less organized and the number of molecules within the outer rings is thus ill defined. This results in larger mobility of the F8H16 molecules in the outer rings and enables molecules to flip orientation.
2) The F8H16 molecules at the center of the aggregate are mostly perpendicular to the surface of water, but become progressively tilted toward the water surface as they move away from the center (Fig. 3). As can be seen, the tilting angle increases monotonically with the distance to the center of the aggregate, but also increases significantly with aggregate size. Simple geometrical arguments show that tilting results from maximizing the occupation of space. The effect is enhanced by the difference in diameter between fluorinated and hydrogenated chains. As the aggregates become larger and the number of rings increases, a limiting value of 90° could be expected for the tilting angle, thus attaining an upper limit for the size of the aggregates, in agreement with experimental observations that report monodispersed objects. The simulation results, however, show that the tilting angle never reaches 90° because the majority of the hydrogenated tails tend to be partially immersed in the water phase, particularly as the clusters get larger.
3) In addition to the tilting angle, which is strictly radial, F8H16 molecules are also oriented tangentially relatively to the rim of the aggregate. This results in a twisted hexagonal arrangement of the molecules, which is clearly visible in the simulations and can be quantified by an azimuthal angle as illustrated in Fig. 4, *Inset.* The simulation results also show that the azimuthal angle gradually decreases, as the aggregates get larger. As for the tilt, the azimuth, and thus the twisted arrangement, is interpreted as a means to minimize the free space between chains, thus maximizing interactions. Due to the trapezoidal shape of the F8H16 molecules, as the aggregates get larger, the number of molecules within the outer rings becomes high enough to maximize occupation of space and interactions, without the need to arrange tangentially. The azimuth thus tends to zero. The molecules are then completely oriented along the radial direction and no twist is observed. Simultaneously, maximum tilt angle is attained. This sets a limit to the size of the aggregates. As can be seen in Fig. 4, for F8H16 aggregates, the simulations predict zero azimuth for aggregates of 31 to 32-nm diameter in excellent agreement with the experimental results, both from AFM (30 ± 1 nm to 35 ± 1.2 nm on solid substrate) and GISAXS (31 ± 7 nm on water subphase).

The side- and cross-section views of the final frame of a simulated 2,500 F8H16 hemimicelle are shown in Fig. 5, together with a topography (AFM-like) image. This is the size of the hemimicelle estimated from experimental observations.

A first confirmation of the ability of the present simulations to describe the experimentally observed hemimicelles of F8H16 and to explain their self-assembly process and stability, is provided by comparing the topography of the simulated and real aggregates. In particular, AFM images of the real systems reveal a depression at the center of the hemimicelles, hence referred to as pit-centered micelles. The formation of this depression has been tentatively explained as the result of curling of long elongated micelles (27). As can be seen in Fig. 5, the simulated aggregates clearly display a depression that closely resembles that

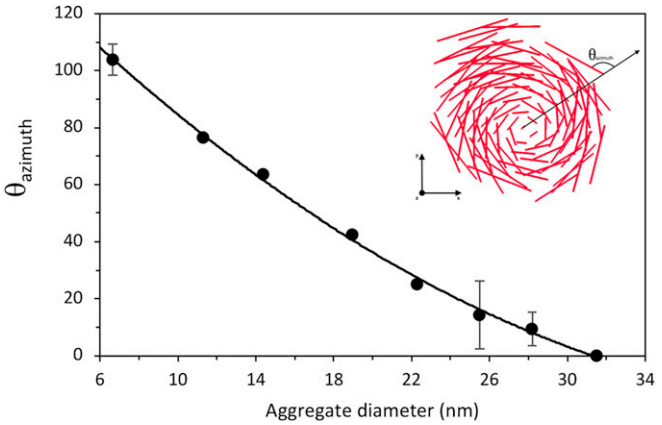

Fig. 4. F8H16 orientation: mean azimuthal angle as a function of micelle size. SDs presented for independent simulations. (*Inset*) The azimuth is defined as the angle between the xy projection of the molecule end-to-end vector and the radius of the aggregate.

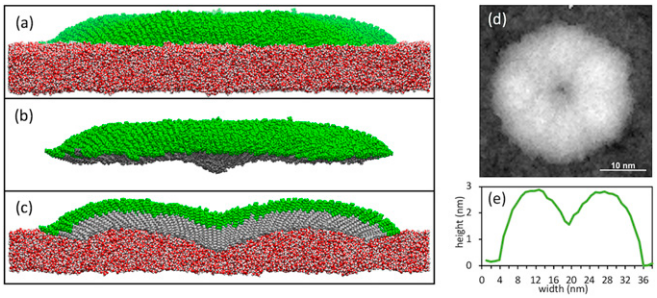

Fig. 5. Different perspectives of the final frame of a simulated hemimicelle with 2500 F8H16 molecules: (*A*) side view; (*B*) side view with water molecules erased to enable visualizing the immersed parts of the aggregate; (*C*) cross-section through the center displaying the internal structure and central depression; (*D*) top-view topography (AFM-like) image depicting a depression in the center (pit-centered micelle); and (*E*) height profile over a cross-section passing through the center of the micelle.

experimentally observed and becomes more noticeable for larger aggregates. Moreover, the existence of this depression in the simulated systems indicates that its formation is not the result of curling of elongated micelles, but intrinsic to the structure of the aggregate. Fig. 5 shows the cross-section of a simulated hemimicelle with 2,500 molecules. The internal structure evidences that the central depression results from plunging of the vertically oriented F8H16 molecules at the center of the aggregate. It can thus be viewed as the collapse of a dome structure at the center of the hemimicelle. The simulations predict a pit depth of 1.4 nm albeit no experimental measurement of the cavity has been rigorously made due to limitations in the tip size inherent to the AFM technique. The thickness of the hemimicelle predicted by the simulations, 3.0 nm, is in excellent agreement within the value obtained by AFM, 3.0 ± 0.1 nm and by GISAXS, 3.8 ± 0.7 nm. This value is lower than the length of a fully stretched F8H16 molecule, as the hydrogenated segments, unlike the fluorinated chains, are partially submerged in the water phase. This is quantitatively confirmed by the density profile of the simulation box (*SI Appendix*, Fig. S1) and is also in agreement with the observation that hemimicelles cannot be observed on dry substrate.

A definite validation of the simulation results was obtained comparing the experimental GIXD spectrum of the system with that calculated from the simulated trajectories. The results are presented in Fig. 6. In the spectrum obtained from the simulated system one clearly observes an in-plane peak at $Q_{xy} = 12.63$ nm^{-1}, which corresponds to the stacking of fluorinated segments and a second one at $Q_{xy} = 14.78$ nm^{-1} associated with the diffraction of hydrogenated blocks. This is in very good agreement with the experimental diffraction spectra presented in Fig. 6*B* which shows a peak at $Q_{xy} = 12.47$ nm^{-1} and a second one at $Q_{xy} = 14.43$ nm^{-1}. The relative intensity of the peaks, I_{fluo}/I_{hydro}, is larger in the simulated spectra than in the experimental (I_{fluo}/I_{hydro} is 2 and 3 for the simulation and experiment, respectively). However, considering that the experimental integration time for acquisition is on the order of a few tenths of a second, this difference can be justified by a larger Debye–Waller factor for the hydrogenated peak. Moreover, the contribution of the hydrogenated segments alone to the GIXD spectra was also calculated from the simulation results (dotted red line in Fig. 6*A*). Two diffraction peaks were obtained, but the one located at $Q_{xy} = 13.2$ nm^{-1} is not detected by the GIXD measurements due to experimental resolution and to the superposition with the fluorinated peak. In conclusion, the complex molecular organization proposed by the MD simulations for the internal structure of the hemimicelles is thus fully validated by the experimental diffraction results. It is noticeable that although the internal micelle's structure is not a real crystal (in the sense that there is no perfect translational properties), it does present "diffraction" peaks in the reciprocal space. This results from the fact that the molecules arrangement can be described algorithmically (the micelles can be then considered as a "pseudocrystal"). In this case, it has been demonstrated that diffraction peaks can be observed as for a 3D quasicrystal.

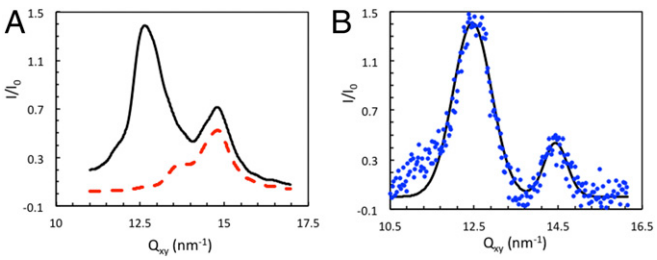

Fig. 6. GIXD of an F8H16 monolayer at 298.15 K from (*A*) MD simulation and (*B*) experiment. Red dotted line is the contribution of the hydrogenated segments alone to the GIXD spectrum.

The simulation results also indicate that there is a minimum number of F8H16 molecules below which the circular aggregates do not form. This hypothesis was tested by removing molecules from the outer rim of 100-molecules hemimicelles. For an aggregate of 90 molecules, circular aggregates still prevail (Fig. 7*B*) but as the number goes down to 60, it collapses into a cylindrical crystal-like block structure made of parallel molecules in a hexagonal packing, partially immersed in water at an average angle of roughly 30° with the water surface (Fig. 7*A*). This indicates that the critical size for the formation of circular aggregates should be between 60 and 90 F8H16 molecules, probably because for a small number of molecules, the contact area between a vertical F8H16 aggregate and water is too low and the circular structure is unstable. These findings about the stability/formation of small aggregates provide important information to understand the mechanism and dynamics of the larger aggregates.

A final argument supports the existence of a limit/optimum size of the hemimicelles: Aggregates smaller than the optimum size should have the tendency to combine/grow forming larger structures, while aggregates close to the optimum size should not. To test this hypothesis, simulations of two identical side-by-side hemimicelles of 100 and 1,763 molecules were performed. We observed that the aggregates of 100 molecules actually do merge into a single hemimicelle within 10 ns, while maintaining the same twisted internal structure. A movie of the merging process is available as *SI Appendix*. In the case of the aggregates of 1,763 molecules no evidence of coalescence was observed, even forcing lateral

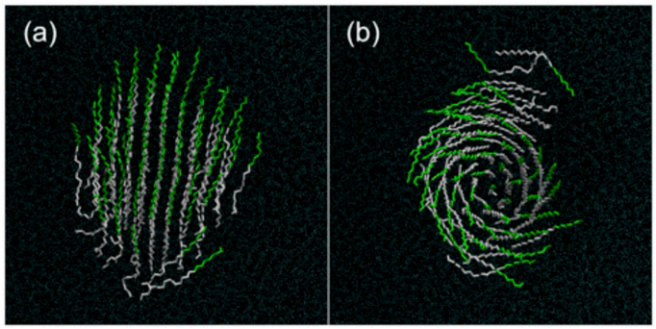

Fig. 7. Top view of the F8H16 clusters with small number of molecules: (*A*) systems with 60 molecules form solid-like block aggregates partially immersed in water; and (*B*) systems with 90 molecules still form circular aggregates displaying the internal twisted organization.

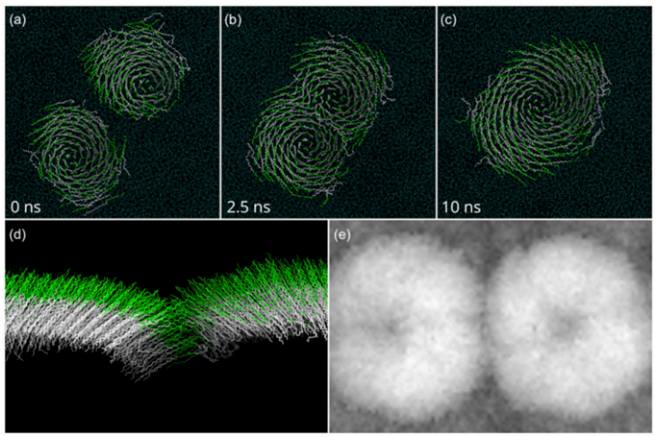

Fig. 8. Testing coalescence of pairs of hemimicelles: (*A*–*C*) top view of two 100-molecules merging hemimicelles in the initial configuration, after 2.5 ns and after 10 ns, respectively; (*D*) side view of the boundary of two 1,763-molecules hemimicelles showing no sign of coalescence; (*E*) topography image of the boundary of the same two 1,763 molecules hemimicelles, showing a slight deformation due to the compression.

compression. Instead of merging together, the aggregates deformed and bent near the boundaries as clearly seen in Fig. 8.

Conclusions

The spontaneous formation of hemimicelles of F8H16 molecules at the surface of water was observed using fully atomistic molecular dynamics simulations. The size and topography of the simulated aggregates closely resemble the experimentally observed hemimicelles.

Furthermore, the GIXD pattern calculated from the simulation trajectories reproduces the experimental GIXD spectra previously obtained, fully validating the MD simulation results.

A detailed inspection of the structure of aggregates with different number of molecules enabled a rational explanation for the spontaneous formation of the aggregates, the aggregation number, and monodispersity experimentally observed.

The F8H16 molecules organize maximizing the occupation of space and interactions, conditioned by a number of key factors: 1) molecular shape, i.e., the relative diameter of the fluorinated and hydrogenated segments, the absolute and relative length of the segments, and their flexibility; 2) the relative hydrophobicity of the fluorinated and hydrogenated segments; 3) the lower surface tension of perfluorinated substances; 4) the specific interaction between the F8H16 dipole and water; and 5) the segregation between fluorinated and hydrogenated segments. Although not periodic, the resulting molecular organization is in agreement with the GIXD measurements.

The use of a force field that was optimized in previous work by modeling a variety of properties of perfluorinated and semifluorinated substances was crucial for achieving the present results.

The MD results indicate that there is a minimum number of F8H16 molecules (<90) needed to form a circular aggregate. Below this number, the molecules form solid-like blocks that can be representative of an early stage of the formation of the hemimicelles.

The topography of the simulated hemimicelles is strikingly similar to those experimentally observed. Even the characteristic depression at the center of the so-called pit-centered micelles is present and thus explained by the simulated aggregates.

The simulations show that aggregates with a number of molecules smaller than the limit can merge to form a larger hemimicelle. Conversely, aggregates with a larger number of molecules than the limit did not merge within the time of simulation.

In this work we have concentrated on exploring and explaining the spontaneous assembly of a single aggregate, an objective that has been fully accomplished. This is an effort to address these highly complex structures and simulating larger systems will be tried in the near future. Results for systems consisting of two (merging and not merging) aggregates are reported and proved to be extremely encouraging.

We believe that the present results can be an important contribution, not only to explain the formation of aggregates of FnHm molecules, but, given the simplicity of the present molecules compared with the common hydrophilic/hydrophobic surfactants, for the understanding of self-assembling processes in general.

Materials and Methods

MD Simulation Details. The systems were modeled using an all-atom force field based on the optimized potentials for liquids simulations (OPLS-AA) (55). Dispersion interactions are modeled with Lennard-Jones potentials centered on each atom and electrostatic interactions are described by atomic partial charges; chemical bonds and angles between adjacent bonds are allowed to move according to harmonic potentials; bond rotations are described by dihedral potentials (truncated cosine series). The fluorinated segment uses the parameters for perfluoroalkanes (56) and the hydrogenated segment the L-OPLS (57) force field for alkanes. Atomic charges of the four carbons closest to the CH_2–CF_2 bond and dihedral functions describing conformations around the fluorinated-hydrogenated junction are from ref. 58. The SPC/E (59) model is used for water molecules. Unlike dispersion interactions are calculated using geometric-mean combining rules, according to OPLS-AA, except for the interactions between hydrogen and fluorine atoms. In this case a factor of 0.77 was applied to the unlike interaction energy ($\varepsilon_{H\text{-}F}$) and a factor of 1.035 to the unlike interaction size ($\sigma_{H\text{-}F}$); these parameters account for the large positive excess volumes and enthalpies of mixtures of alkanes with perfluoroalkanes (52).

Simulations were performed using the GROMACS 5.0.7 code (60) with 2-fs time steps and the leapfrog algorithm, constraining bonds which include hydrogen atoms to their equilibrium lengths with the LINCS algorithm (61). A cutoff of 1.4 nm and particle-mesh Ewald calculations were used for both dispersion and electrostatic interactions. Production runs were done in the NVT ensemble at 298.15 K using the velocity-rescaling thermostat (modification of the Berendsen algorithm) with 0.5-ps coupling constant (62).

For the construction of the simulation systems, 2 tetragonal simulation boxes were built, one with 10,000 and the other with 17,500 water molecules. The geometry of the boxes (9.1 × 9.1 × 15 nm and 13 × 13 × 15 nm, respectively) was chosen to generate a water slab with a thickness around 3.5 nm and two explicit liquid–vapor interfaces, perpendicular to the *z* axis. These systems were equilibrated for at least 3 ns in the NVT ensemble, with periodic boundary conditions in all directions. All subsequent simulations were built from these 2 equilibrated water slabs, which were replicated in the x-y plane whenever a larger water surface was needed. The initial coordinates were generated using the Packmol (63) software. The height (z dimension) of the simulation boxes was chosen to ensure that no significant interactions were felt between the periodic replicas in the z direction. The x and y dimensions were chosen large enough to prevent interaction between the periodic images of the PFAA aggregates. MD simulations starting from vertically aligned molecules led to aggregates structurally identical to those obtained from randomly initialized runs. The convergence of these simulations occurs in a timeframe 2 orders of magnitude shorter than the ones starting from a random configuration. Thus, for larger aggregates, initial configurations with vertically aligned molecules were used. The simulations ran for at least 10 ns and it was verified that the properties remained constant during the latter 2 ns.

ACKNOWLEDGMENTS. We acknowledge funding from Fundação para a Ciência e Tecnologia (FCT) through the project UID/QUI/0100/2013. P.M. acknowledges funding from FCT, Postdoctoral Grant SFRH/BPD/81748/2011. G.M.C.S. acknowledges funding from FCT, Grant SFRH/BD/123565/2016.

1. B. P. Binks, P. D. I. Fletcher, S. N. Kotsev, R. L. Thompson, Adsorption and aggregation of semifluorinated alkanes in binary and ternary mixtures with hydrocarbon and fluorocarbon solvents. *Langmuir* **13**, 6669–6682 (1997).
2. W. Mahler, D. Guillon, A. Skoulios, Smectic liquid-crystal from (perfluorododecyl) decane. *Mol. Cryst. Liq. Cryst. (Phila. Pa.)* **2**, 111–119 (1985).
3. C. Viney, T. P. Russell, L. E. Depero, R. J. Twieg, Transitions to liquid-crystalline phases in a semifluorinated alkane. *Mol. Cryst. Liq. Cryst. (Phila. Pa.)* **168**, 63–82 (1989).
4. C. Viney, R. J. Twieg, T. P. Russell, L. E. Depero, The structural basis of transitions between highly ordered smectic phases in semifluorinated alkanes. *Liq. Cryst.* **5**, 1783–1788 (1989).

5. J. G. Riess, Fluorous micro- and nanophases with a biomedical perspective. *Tetrahedron* **58**, 4113–4131 (2002).
6. J. G. Riess, Highly fluorinated amphiphilic molecules and self-assemblies with biomedical potential. *Curr. Opin. Colloid Interface Sci.* **14**, 294–304 (2009).
7. H. Meinert, T. Roy, Semifluorinated alkanes - a new class of compounds with outstanding properties for use in ophthalmology. *Eur. J. Ophthalmol.* **10**, 189–197 (2000).
8. P. Steven *et al*., Semifluorinated alkane eye drops for treatment of dry eye disease–A prospective, multicenter noninterventional study. *J. Ocul. Pharmacol. Ther.* **31**, 498–503 (2015).
9. F. Gerber, M. P. Krafft, T. F. Vandamme, M. Goldmann, P. Fontaine, Preventing crystallization of phospholipids in monolayers: A new approach to lung-surfactant therapy. *Angew. Chem. Int. Ed. Engl.* **44**, 2749–2752 (2005).
10. J. G. Riess, M. P. Krafft, Elaboration of fluorocarbon emulsions with improved oxygen-carrying capabilities. *Adv. Exp. Med. Biol.* **317**, 465–472 (1992).
11. F. Gerber, M. P. Krafft, T. F. Vandamme, M. Goldmann, P. Fontaine, Fluidization of a dipalmitoyl phosphatidylcholine monolayer by fluorocarbon gases: Potential use in lung surfactant therapy. *Biophys. J.* **90**, 3184–3192 (2006).
12. M. P. Krafft, Overcoming inactivation of the lung surfactant by serum proteins: A potential role for fluorocarbons? *Soft Matter* **11**, 5982–5994 (2015).
13. T. Nardin *et al*., Elaboration of porous silicon carbide by soft templating molecular precursors with semi-fluorinated alkanes. *J. Mater. Chem. A* **3**, 3082–3090 (2015).
14. C. G. Clark, Jr, *et al*., Molecularly tethered amphiphiles as 3-D supramolecular assembly platforms: Unlocking a trapped conformation. *J. Am. Chem. Soc.* **131**, 8537–8547 (2009).
15. V. Percec *et al*., Self-assembly of semifluorinated janus-dendritic benzamides into bilayered pyramidal columns. *Angew. Chem. Int. Ed. Engl.* **44**, 4739–4745 (2005).
16. P. Riachy *et al*., Investigation of a novel fluorinated surfactant-based system for the design of spherical wormhole-like mesoporous silica. *J. Colloid Interface Sci.* **487**, 310–319 (2017).
17. E. A. Chavez Panduro *et al*., Nonionic fluorinated surfactant removal from mesoporous film using sc-CO_2. *ACS Appl. Mater. Interfaces* **9**, 3093–3101 (2017).
18. J. F. Rabolt, T. P. Russell, R. J. Twieg, Structural studies of semifluorinated N-alkanes. 1. Synthesis and characterization of F(CF2)n(CH2)mH in the solid state. *Macromolecules* **17**, 2786–2794 (1984).
19. T. P. Russell, J. F. Rabolt, R. J. Twieg, R. L. Siemens, B. L. Farmer, Structural characterization of semifluorinated N-alkanes. 2. Solid-solid transition behavior. *Macromolecules* **19**, 1135–1143 (1986).
20. J. Höpken, M. Möller, On the morphology of (perfluoroalkyl)alkanes. *Macromolecules* **25**, 2482–2489 (1992).
21. P. Marczuk, P. Lang, A structural X-ray study on semifluorinated alkanes (SFA): SFA revisited. *Macromolecules* **31**, 9013–9018 (1998).
22. C. Tsagogiorgas *et al*., Semifluorinated alkanes–A new class of excipients suitable for pulmonary drug delivery. *Eur. J. Pharm. Biopharm.* **76**, 75–82 (2010).
23. M. P. Turberg, J. E. Brady, Semifluorinated hydrocarbons–Primitive surfactant molecules. *J. Am. Chem. Soc.* **110**, 7797–7801 (1988).
24. M. Maaloum, P. Muller, M. P. Krafft, Monodisperse surface micelles of nonpolar amphiphiles in langmuir monolayers. *Angew. Chem. Int. Ed. Engl.* **41**, 4331–4334 (2002).
25. A. L. Simões Gamboa, E. J. M. Filipe, P. Brogueira, Nanoscale pattern formation in Langmuir-Blodgett films of a semifluorinated alkane and a polystyrene-poly(ethylene oxide) diblock copolymer. *Nano Lett.* **2**, 1083–1086 (2002).
26. G. Zhang, M. Maaloum, P. Muller, N. Benoit, M. P. Krafft, Surface micelles of semifluorinated alkanes in Langmuir–Blodgett monolayers. *Phys. Chem. Chem. Phys.* **6**, 1566–1569 (2004).
27. G. Zhang *et al*., Occurrence, shape, and dimensions of large surface hemimicelles made of semifluorinated alkanes. Elongated versus circular hemimicelles. Pit- and tip-centered hemimicelles. *J. Am. Chem. Soc.* **127**, 10412–10419 (2005).
28. C. Schwieger, X. Liu, M. P. Krafft, Self-assembled mesoscopic surface domains of fluorocarbon-hydrocarbon diblocks can form at zero surface pressure: Tilting of solid-like hydrocarbon moieties compensates for cross-section mismatch with fluorocarbon moieties. *Phys. Chem. Chem. Phys.* **19**, 23809–23816 (2017).
29. P. Fontaine *et al*., Direct evidence for highly organized networks of circular surface micelles of surfactant at the air-water interface. *J. Am. Chem. Soc.* **127**, 512–513 (2005).
30. L. Bardin *et al*., Long-range nanometer-scale organization of semifluorinated alkane monolayers at the air/water interface. *Langmuir* **27**, 13497–13505 (2011).
31. M. Veschgini *et al*., Size, shape, and lateral correlation of highly uniform, mesoscopic, self-assembled domains of fluorocarbon-hydrocarbon diblocks at the air/water interface: A GISAXS study. *ChemPhysChem* **18**, 2791–2798 (2017).
32. M. P. Krafft, Large organized surface domains self-assembled from nonpolar amphiphiles. *Acc. Chem. Res.* **45**, 514–524 (2012).
33. P. Fontaine, M. C. Fauré, L. Bardin, E. J. M. Filipe, M. Goldmann, Evidence for interaction with the water subphase as the origin and stabilization of nano-domain in semi-fluorinated alkanes monolayer at the air/water interface. *Langmuir* **30**, 15193–15199 (2014).
34. C. de Gracia Lux, J. L. Gallani, G. Waton, M. P. Krafft, Stacking of self-assembled surface micelles in ultrathin films. *ChemPhysChem* **13**, 1454–1462 (2012).
35. C. de Gracia Lux, J. L. Gallani, G. Waton, M. P. Krafft, Compression of self-assembled nano-objects: 2D/3D transitions in films of (perfluoroalkyl)alkanes–Persistence of an organized array of surface micelles. *Chemistry* **16**, 7186–7198 (2010).
36. X. Liu *et al*., 2D spherulites of a semi-fluorinated alkane: Controlled access to either radial or ring-banded morphologies. *ChemPhysChem* **19**, 29–33 (2018).
37. A. N. Semenov, A. González-Pérez, M. P. Krafft, J.-F. Legrand, Theory of surface micelles of semifluorinated alkanes. *Langmuir* **22**, 8703–8717 (2006).
38. A. Mourran *et al*., Self-assembly of the perfluoroalkyl-alkane F14H20 in ultrathin films. *Langmuir* **21**, 2308–2316 (2005).
39. L. Bardin, M. C. Faure, E. J. M. Filipe, P. Fontaine, M. Goldmann, Highly organized crystalline monolayer of a semi-fluorinated alkane on a solid substrate obtained by spin-coating. *Thin Solid Films* **519**, 414–416 (2010).
40. X. Feng, A. Mourran, M. Möller, C. Bahr, AFM study of Gibbs films of semifluorinated alkanes at liquid crystal/air interfaces. *ChemPhysChem* **14**, 1801–1805 (2013).
41. O. Gang *et al*., Surface phases of semi-fluorinated alkane melts. *Europhys. Lett.* **49**, 761–767 (2000).
42. A. Piñeiro, G. Prieto, J. M. Ruso, P. V. Verdes, F. Sarmiento, Surface films of short fluorocarbon-hydrocarbon diblocks studied by molecular dynamics simulations: Spontaneous formation of elongated hemimicelles. *J. Colloid Interface Sci.* **329**, 351–356 (2009).
43. P. Morgado, G. Das, C. McCabe, E. J. M. Filipe, Vapor pressure of perfluoroalkylalkanes: The role of the dipole. *J. Phys. Chem. B* **119**, 1623–1632 (2015).
44. P. Morgado, "Semifluorinated alkanes - structure properties relationships," PhD thesis, Instituto Superior Técnico, Lisboa (2011).
45. P. Morgado *et al*., Liquid phase behavior of perfluoroalkylalkane surfactants. *J. Phys. Chem. B* **111**, 2856–2863 (2007).
46. P. Morgado *et al*., Systems involving hydrogenated and fluorinated chains: Volumetric properties of perfluoroalkanes and perfluoroalkylalkane surfactants. *J. Phys. Chem. B* **115**, 15013–15023 (2011).
47. P. Morgado *et al*., Viscosity of liquid perfluoroalkanes and perfluoroalkylalkane surfactants. *J. Phys. Chem. B* **115**, 9130–9139 (2011).
48. P. Morgado *et al*., SAFT-γ force field for the simulation of molecular fluids: 8. heterosegmented coarse-grained models of perfluoroalkylalkanes assessed with new vapour–liquid interfacial tension data. *Mol. Phys.* **114**, 2597–2614 (2016).
49. P. Morgado *et al*., Solution behavior of perfluoroalkanes and perfluoroalkylalkane surfactants in N-octane. *J. Phys. Chem. C* **111**, 15962–15968 (2007).
50. P. Morgado, H. Rodrigues, F. J. Blas, C. McCabe, E. J. M. Filipe, Perfluoroalkanes and perfluoroalkylalkane surfactants in solution: Partial molar volumes in n-octane and hetero-SAFT-VR modelling. *Fluid Phase Equilib.* **306**, 76–81 (2011).
51. P. Morgado *et al*., Liquid mixtures involving hydrogenated and fluorinated alcohols: Thermodynamics, spectroscopy, and simulation. *J. Phys. Chem. B* **120**, 10091–10105 (2016).
52. P. Morgado, A. R. Garcia, L. F. G. Martins, L. M. Ilharco, E. J. M. Filipe, Alkane coiling in perfluoroalkane solutions: A new primitive solvophobic effect. *Langmuir* **33**, 11429–11435 (2017).
53. L. de Viguerie *et al*., Effect of the molecular structure on the hierarchical self-assembly of semifluorinated alkanes at the air/water interface. *Langmuir* **27**, 8776–8786 (2011).
54. M. Broniatowski, J. Miñones, Jr, P. Dynarowicz-Łatka, Semifluorinated chains in 2D-(perfluorododecyl)-alkanes at the air/water interface. *J. Colloid Interface Sci.* **279**, 552–558 (2004).
55. W. L. Jorgensen, D. S. Maxwell, J. Tirado-Rives, Development and testing of the OLPS all-atom force field on conformational energetics and properties of organic liquids. *J. Am. Chem. Soc.* **118**, 11225–11236 (1996).
56. E. K. Watkins, W. L. Jorgensen, Perfluoroalkanes: Conformational analysis and liquid-state properties from ab initio and Monte Carlo calculations. *J. Phys. Chem. A* **105**, 4118–4125 (2001).
57. S. W. I. Siu, K. Pluhackova, R. A. Böckmann, Optimization of the OPLS-AA force field for long hydrocarbons. *J. Chem. Theory Comput.* **8**, 1459–1470 (2012).
58. A. A. H. Pádua, Torsion energy profiles and force fields derived from ab initio calculations for simulations of hydrocarbon-fluorocarbon diblocks and perfluoroalkylbromides. *J. Phys. Chem. A* **106**, 10116–10123 (2002).
59. H. J. C. Berendsen, J. R. Grigera, T. P. Straatsma, The missing term in effective pair potentials. *J. Phys. Chem.* **91**, 6269–6271 (1987).
60. D. Van Der Spoel *et al*., GROMACS: Fast, flexible, and free. *J. Comput. Chem.* **26**, 1701–1718 (2005).
61. B. Hess, H. Bekker, H. J. C. Berendsen, J. G. E. M. Fraaije, LINCS: A linear constraint solver for molecular simulations. *J. Comput. Chem.* **18**, 1463–1472 (1997).
62. G. Bussi, D. Donadio, M. Parrinello, Canonical sampling through velocity rescaling. *J. Chem. Phys.* **126**, 014101 (2007).
63. L. Martínez, R. Andrade, E. G. Birgin, J. M. Martínez, PACKMOL: A package for building initial configurations for molecular dynamics simulations. *J. Comput. Chem.* **30**, 2157–2164 (2009).